Cloud Detection with MODIS. Part I: Improvements in the MODIS Cloud Mask for Collection 5

RICHARD A. FREY, STEVEN A. ACKERMAN, YINGHUI LIU, KATHLEEN I. STRABALA, HONG ZHANG, JEFFREY R. KEY, AND XUANGI WANG

Cooperative Institute for Meteorological Satellite Studies, University of Wisconsin—Madison, Madison, Wisconsin

(Manuscript received 20 August 2007, in final form 9 January 2008)

ABSTRACT

Significant improvements have been made to the Moderate Resolution Imaging Spectroradiometer (MODIS) cloud mask (MOD35 and MYD35) for Collection 5 reprocessing and forward stream data production. Most of the modifications are realized for nighttime scenes where polar and oceanic regions will see marked improvement. For polar night scenes, two new spectral tests using the 7.2-μm water vapor absorption band have been added as well as updates to the 3.9–12- and 11–12-μm cloud tests. More non-MODIS ancillary input data have been added. Land and sea surface temperature maps provide crucial information for mid- and low-level cloud detection and lessen dependence on ocean brightness temperature variability tests. Sun-glint areas are also improved by use of sea surface temperatures to aid in resolving observations with conflicting cloud versus clear-sky signals, where visible and near-infrared (NIR) reflectances are high, but infrared brightness temperatures are relatively warm. Day and night Arctic cloud frequency results are compared to those created by the Advanced Very High Resolution Radiometer (AVHRR) Polar Pathfinder-Extended (APP-X) algorithm. Day versus night sea surface temperatures derived from MODIS radiances and using only the MODIS cloud mask for cloud screening are contrasted. Frequencies of cloud from sun-glint regions are shown as a function of sun-glint angle to gain a sense of cloud mask quality in those regions. Continuing validation activities are described in Part II of this paper.

1. MODIS cloud mask overview

The Moderate Resolution Imaging Spectroradiometer (MODIS) is a key instrument of the Earth Observing System (EOS). It measures radiances at 36 wavelengths including infrared and visible bands with spatial resolution of 250 m–1 km. Earth Observing System models require knowledge of whether a radiance profile is cloud free. If the profile is not cloud free, it is valuable to have information concerning the type of cloud. Cloud mask algorithms for MODIS that use a series of sequential tests on the radiances or their associated brightness temperatures may be found in Ackerman et al. (1998), King et al. (2003), and Platnick et al. (2003), where their description as part of the MODIS Cloud Products Suites is described.

Cloud detection is based on the contrast (i.e., cloud versus background surface) in a given target area—in this case, a 1-km (at nadir) pixel. Contrast may be defined as differing signals for individual spectral bands (e.g., clouds are generally more reflective in the visible but colder than the background as measured in the thermal IR), spectral combinations (e.g., 0.86-/0.66-μm ratio is close to unity for cloudy skies), or temporal and spatial variations of these. The MODIS cloud mask uses several cloud detection tests to indicate a level of confidence that MODIS is observing a clear-sky scene. Produced for the entire globe, day and night, and at 1-km resolution, the cloud mask algorithm employs up to 14 MODIS spectral bands (250- and 500-m band radiances aggregated to 1 km) to maximize reliable cloud detection. In addition, a 250-m mask derived from the two 250-m-resolution bands (0.65 and 0.86 μm) in combination with 1-km cloud mask results is produced and archived, but will not be discussed here. The 1-km mask is independent of the 250-m mask.

The cloud mask assesses the likelihood that clouds obstruct a given pixel. As cloud cover can occupy a pixel to varying extents, the MODIS cloud mask is de-

Corresponding author address: Richard A. Frey, CIMSS, University of Wisconsin—Madison, 1225 W. Dayton St., Madison, WI 53706.
E-mail: richard.frey@ssec.wisc.edu

DOI: 10.1175/2008JTECHA1052.1

signed to allow for varying degrees of clear-sky confidence (i.e., it provides more information than a simple yes/no decision). To assist users in interpreting the results, the cloud mask consists of 48 bits of output per pixel that include information on individual cloud test results, the processing path, and ancillary information (e.g., land/sea tag). In addition, the first eight bits of the cloud mask provide a summary adequate for many processing applications. Further, the first two bits of the mask summarize the results from all individual tests by classifying cloud contamination in every pixel of data as either confident clear, probably clear, uncertain/probably cloudy, or cloudy.

The MODIS cloud mask algorithm identifies several conceptual domains according to surface type and solar illumination including land, water, snow/ice, desert, and coast for both day and night. Once a pixel is assigned to a particular domain (defining an algorithm path), a series of threshold tests attempts to detect the presence of clouds or optically thick aerosol in the instrument field of view. Each test returns a confidence level that the pixel is clear ranging in value from 1 (high-confidence clear) to 0 (very low-confidence clear or high confidence of cloud or other obstruction). Ackerman et al. (1998) provide details of confidence calculations for individual spectral tests. There are several types of tests, where detection of various cloud conditions relies on different sets of tests. Those capable of detecting similar cloud conditions are grouped together. While these groups are arranged so that independence between them is maximized, few, if any, spectral tests are completely independent. As described by Ackerman et al. (1998), a minimum confidence is determined for each group as follows:

$$G_{j=1-N} = \min[F_{(i,j)}]_{i=1-m}, \tag{1}$$

where $F_{i,j}$ is the confidence level of an individual spectral test, m is the number of tests in a given group, j is the group index, and N is the number of groups (e.g., 5). The final cloud mask confidence (Q) is then determined from the products of the results for each group,

$$Q = \sqrt[N]{\prod_{i=1}^{N} G_j}. \tag{2}$$

The four confidence levels included in the cloud mask output are (i) confident clear ($Q > 0.99$); (ii) probably clear ($Q > 0.95$); (iii) uncertain/probably cloudy ($Q > 0.66$); and (iv) cloudy ($Q \leq 0.66$). These outcomes constitute bits 1 and 2 of the mask. Note that the result gives the confidence, or lack thereof, in the existence of a clear pixel and not the confidence in the presence of an overcast cloudy pixel. As such, the *cloudy* outcome can alternately be labeled as *not clear* (i.e., high confidence in an obstruction in the field of view).

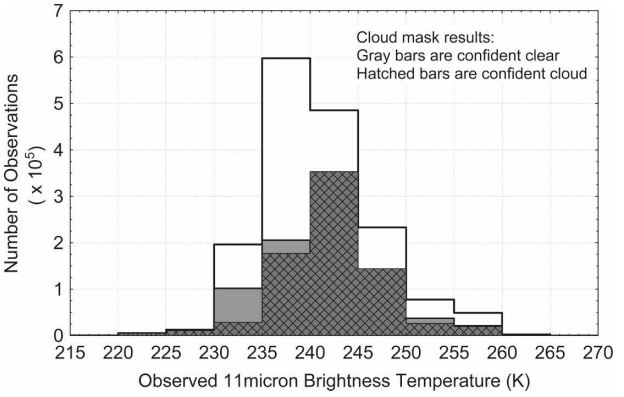

FIG. 1. Histogram of 11-μm BTs over frozen ocean from 1 Jan 2003 near the North Pole.

This approach is clear-sky conservative in the sense that if any test is highly confident that a scene is cloudy ($F_{i,j} = 0$), the final clear-sky confidence is also 0. However, it is also the case that the overall mask cannot be clear-sky conservative if individual test thresholds are set to flag only thick cloud or overcast conditions. Therefore, thresholds are set so that they detect the maximum number of cloudy pixels without generating unacceptably large numbers of "false alarms" (clear pixels incorrectly flagged as cloudy). Though an attempt has been made to represent regional and global cloud fractions by aggregating pixels flagged as either cloudy or probably cloudy, we recognize that some users may need more detail. For example, a reasonably accurate estimate of high-cloud frequency may be obtained by counting only those pixels for which high-cloud tests are positive. Much detailed information is contained in Ackerman et al. (2006) and the MODIS Cloud Mask User's Guide (available online at http://cimss.ssec.wisc.edu/modis1/pdf/CMUSERSGUIDE.PDF).

2. Cloud mask enhancements

a. Polar night

Discriminating clear-sky from cloudy conditions is nowhere more difficult than in conditions of polar night. Also, verifying cloud detection results in polar night conditions is very difficult without human observations or active sensors with which to compare. Both are almost totally absent during polar winter. Figure 1 shows both the underlying problem in cloud detection for polar night and an indication of cloud mask results. It shows a histogram of observed brightness tempera-

tures (BTs) from one MODIS granule (open bars) over frozen ocean near the North Pole. Also shown are the amounts of confident clear and confident cloudy retrievals for each BT class. Instead of clear-sky observations making a distinct peak on the warm end of the histogram as in most earth scenes, this shows a more Gaussian distribution with most values (both clear and cloudy) somewhere in the middle. However, as shown in the figure, in a given region one expects temperatures and water vapor loading in clear skies over the surface ice to be relatively uniform so that a majority of those BTs will fall in one 5-K-wide class. This was verified by inspection of the imagery for this granule. Note that many, if not most, of the confident cloudy BTs were in either the same or warmer BT classes as that of the clear-sky peak, indicating the lack of thermal contrast that is the fundamental cloud detection problem for polar night. Liu et al. (2004) compared ground-based radar/lidar data to MODIS cloud mask results using the new polar night spectral tests [included in the cloud mask algorithm for Collection 5 (C5)] and those from Collection 4 (previous operational version) and found that the misidentification rate of cloud as clear decreased from 44.2% to 16.3% at two Arctic stations. The misidentification of clear as cloud remained at about 8%. In Collection 5 of the MODIS cloud mask, two spectral cloud tests were modified, two were added, and one clear-sky restoral (CSR) test was added when processing polar night scenes.

1) THE 11–3.9-μM BTD LOW CLOUD TEST

The 11–3.9-μm brightness temperature difference (BTD) low cloud test is based on the differential absorption between these two wavelengths by both water and ice cloud particles. The nighttime BTD may be either negative or positive depending on cloud optical depth and particle size (Liu et al. 2004). However, the situation becomes more complex in temperature inversions that are frequent in polar night conditions. For a complete discussion of the problem, see Liu et al. (2004). Previous 11–3.9-μm test thresholds did not take temperature inversions into account and were most appropriate for nonpolar, thick water clouds. For Collection 5, the high-confident cloud thresholds vary linearly from -0.8 to $+0.6$ as the 11-μm BT varies between 235 and 265 K. The threshold is constant below 235 and above 265 K. Figure 2b shows an example of test results on 1 April 2003 beginning at 0505 UTC from northwestern Canada. Figure 2a shows imagery of MODIS 11-μm BTs for the same scene. Note that north is at the bottom and west is to the right in these images. In all test result figures, white means cloud indicated, gray means no cloud indicated, and black means test not performed.

2) THE 3.9–12-μM BTD HIGH CLOUD TEST

The 3.9–12-μm BTD high cloud test has been modified for polar night conditions. For reasons not well understood, the thresholds for this test need to be increased with decreasing temperatures below 265 K. This is counterintuitive from arguments based on atmospheric water vapor loading and absorption at these two wavelengths. Perhaps the calibration of one or both bands is of reduced accuracy at cold temperatures. In addition, the test cannot be used on the very coldest and driest scenes (surface elevations greater than 2000 m) such as are found in Antarctica and Greenland during the winter season. Therefore, the test is not performed in polar night conditions when the elevation exceeds 2000 m. The Collection 5 confident cloud threshold varies linearly from $+4.5$ to $+2.5$ K as the 11-μm BT varies between 235 and 265 K. The threshold is constant below 235 and above 265 K. Figure 2d shows an example of test results from the same scene as above.

3) THE 11–12-μM BTD THIN CIRRUS TEST

Previous versions of the cloud mask algorithm made use of this test only over surfaces not covered by snow or ice. The Collection 5 test makes use of thresholds taken from Key (2002), who extended the Saunders and Kriebel (1988) values to very low temperatures. The modified test has replaced the original in all processing paths for both day and night processing except for Antarctica. Figure 2c shows example results from the same scene as above. At these very cold scene temperatures, the 11–12-μm BTD starts to become noisy (as seen at middle left).

4) THE 7.2–11-μM BTD CLOUD TEST

The most significant change to the polar night algorithm is the addition of a new 7.2–11-μm BTD cloud test. Since the weighting function of the 7.2-μm band peaks at about 800 hPa, the BTD is related to the temperature difference between the 800-hPa layer and the surface, which the 11-μm band is most sensitive to. In the presence of low clouds under polar night conditions with a temperature inversion, radiation from the 11-μm band comes primarily from the relatively warm cloud top, decreasing the 7.2–11-μm BTD compared to the clear-sky value. In conditions of deep polar night, even high clouds may be warmer than the surface and will often be detected with this test. For middle and high

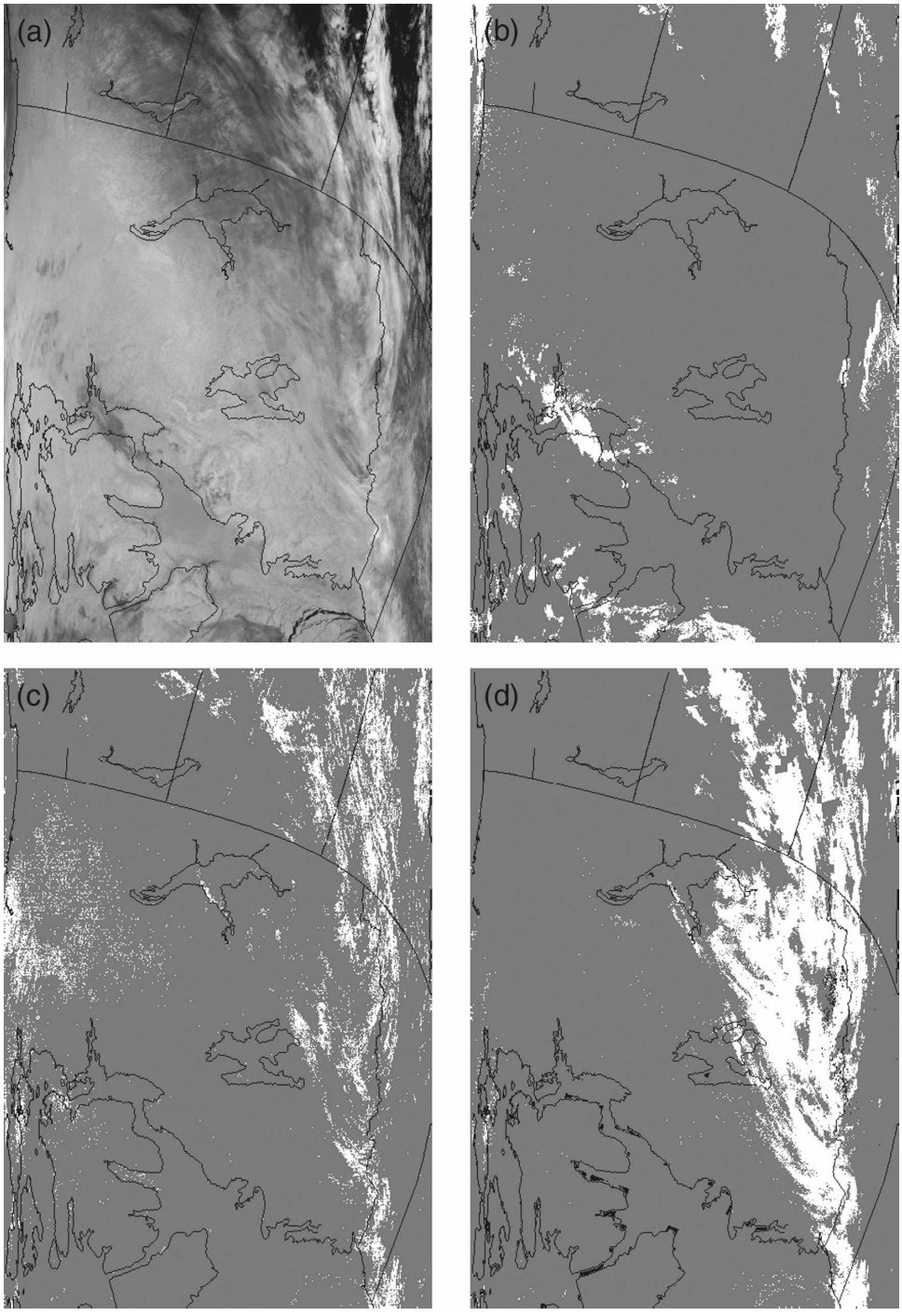

FIG. 2. (a) MODIS 11-μm BT image, (b) 11–3.9-μm BTD test, (c) 11–12-μm BTD test, and (d) 3.9–12-μm BTD test. Scene is from 0505 UTC 1 Apr 2003.

clouds in an atmosphere with no inversion, the BTD is lessened because both the 11- and 7.2-μm radiances are emanating from near cloud top with little water vapor attenuation in the 7.2-μm band in the dry polar atmosphere. For a complete discussion of the theory, see Liu et al. (2004). The test as configured in MOD35 is applicable only over nighttime snow and ice surfaces. Because the 7.2-μm band is sensitive to atmospheric water vapor and also because inversion strength tends to increase with decreasing surface temperatures over snow-

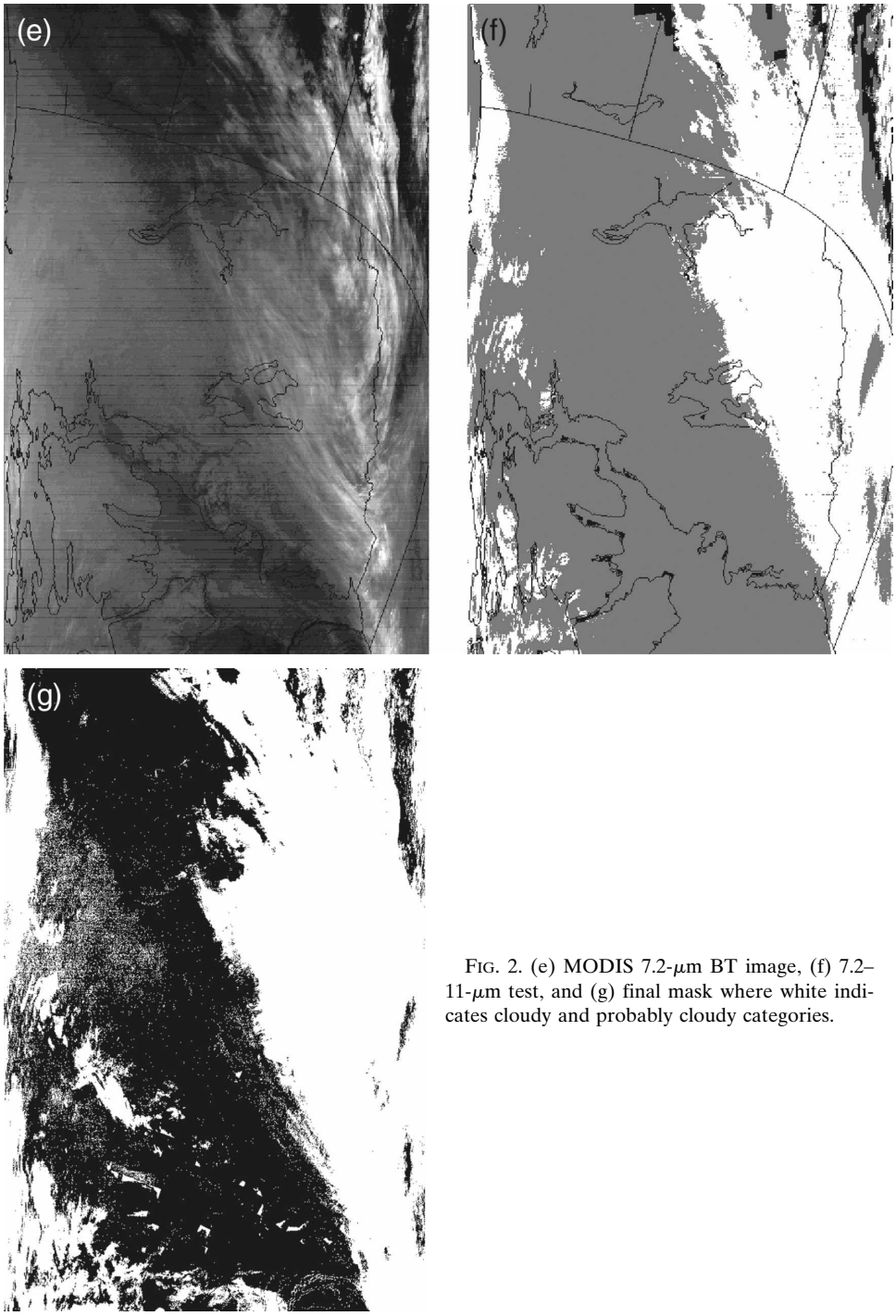

FIG. 2. (e) MODIS 7.2-μm BT image, (f) 7.2–11-μm test, and (g) final mask where white indicates cloudy and probably cloudy categories.

covered land (Liu et al. 2004), thresholds for this test are a function of the observed 11-μm BT. The thresholds vary linearly in three ranges: BTD + 2 to −4.5 K for 11 μm between 220 and 245 K, BTD −4.5 to −11.5 K for 11 μm between 245 and 255 K, and BTD −11.5 to −21 K for 11-μm between 255 and 265 K. Thresholds are constant for 11 μm below 220 or above 265 K. The thresholds are slightly different over ice (frozen water surfaces): BTD + 2 to −4.5 K for 11 μm between 220 and 245 K, BTD −4.5 to −17.5 K for 11 μm between 245 and 255 K, and BTD −17.5 to −21 K for 11 μm between 255 and 265 K. These somewhat larger BTDs presumably reflect a lesser tendency for strong inversions and higher water vapor loading over frozen water

surfaces as opposed to snow-covered land areas. These thresholds also differ slightly from those reported in Liu et al. (2004), a result of extensive testing over many scenes and the necessity of meshing this test with other cloud mask tests and algorithms. Note that this test was also implemented for nonpolar (latitude $<60°$), nighttime snow-covered land. Figure 2e shows imagery from the 7.2-μm band for this same scene from Canada and Fig. 2f shows the results of the test. Note the difference in texture between cloudy and clear on the right in the 7.2-μm BT imagery, even though the gray-scale indicates similar temperatures for much of the scene. Clouds indicated on the left are just barely seen in Fig. 2a.

5) THE 7.2–11-μM BTD CLEAR-SKY TEST

The MODIS cloud mask employs several spectral tests that attempt to identify unambiguously clear pixels in polar night conditions. Positive results override any cloud indications. A 7.2–11-μm BTD test may be utilized to find clear sky because of the prevalence of polar night temperature inversions. This test works in the same way as the current 6.7–11-μm BTD clear-sky restoral test, where 11-μm BTs are sometimes significantly lower than those measured in the 6.7-μm band because the 6.7-μm weighting function peaks near the top of a warmer inversion layer in some cases. However, since the 7.2-μm band peaks lower in the atmosphere, a 7.2–11-μm BTD test can detect lower and weaker inversions. Pixels are restored to clear if the 7.2–11-μm BTD > 5 K.

b. Polar daytime snow

A new version of the 3.9–11-μm test has been developed for polar daytime conditions. The test thresholds are now dependent on the observed 11-μm BT when that BT is lower than 245 K. Also, the test will no longer be performed at all when the 11-μm BT is below 230 K. During Arctic and Antarctic spring and autumn seasons, the sun is above the horizon but surface temperatures and hence clear-sky observed BTs are still very low, sometimes <200 K at 11 μm on the Antarctic Plateau near the South Pole. Under these conditions, and adding just a small amount of solar insolation, the extreme nonlinearity of the Planck function at 3.9 μm makes the 3.9–11-μm BTD higher than one would expect for clear-sky observations at warmer temperatures. This effect, along with the use of static test thresholds, was leading to false cloud determinations in Antarctica and Greenland. The new thresholds will vary between 7.0 and 14.5 K as 11-μm BTs vary between 245 and 230 K at the 0.5 clear-sky confidence level. Above 245 K, the threshold will remain as before, at 7 K.

c. Arctic cloud frequency comparisons

Figures 3a–f show mean Arctic cloud frequencies from *Aqua* MODIS Collection 5 cloud mask and AVHRR Polar Pathfinder-Extended (APP-X) (Key 2002) data and differences between them during day and night for the period January 2003–December 2004. MODIS cloud amounts are generally higher than APP-X during daytime (warm season), especially in northern Canada, Siberia, and Greenland. At night (cold season), differences are generally smaller except for some portions of Greenland's eastern coast and the Canadian archipelago. Figure 4 shows time series of monthly mean cloud frequencies for the two datasets, day and night separately. Note that from May through September, the daytime values compare very well, then diverge rapidly as polar darkness descends. At night, December through April values are quite similar. The Warren et al. (1986, 1988) values for day and night together are shown (black line) for reference. Distributions of MODIS minus APP-X cloud fractions for day (blue curve) and night (red curve) are shown in Fig. 5. Greater uncertainty between the two datasets is expected during nighttime conditions due to less available information delineating clear skies from cloudy. The mode is +5%.

d. Nighttime land

The major enhancement to nighttime land processing is the inclusion of a surface temperature (SFCT) test. Gridded surface air temperatures from Global Data Assimilation System (GDAS) model output fields (Derber et al. 1991) are compared to observed 11-μm BTs. Because of large variations of SFCT in mountainous areas and large diurnal swings in desert regions that are not always well characterized in the gridded data, the test is not performed there. Even with these restrictions, great care must be taken when applying this test. Thresholds of GDAS SFCT minus 11-μm BT are set at 12 K for vegetated areas and 20 K for semiarid lands but are adjusted for viewing zenith angle (VZA) and water vapor loading based on 11–12-μm BTDs. The basic thresholds are increased by 2 times the 11–12-μm BTD and nonlinearly with viewing zenith angle, from 0 K at nadir to a maximum of 3 K at the edge of the scan. With threshold values set this high, the test can obviously function only as a gross cloud test. But it is particularly useful for detecting thick midlevel clouds that are surprisingly difficult to detect at night over land. The test is also performed on snow-free polar scenes.

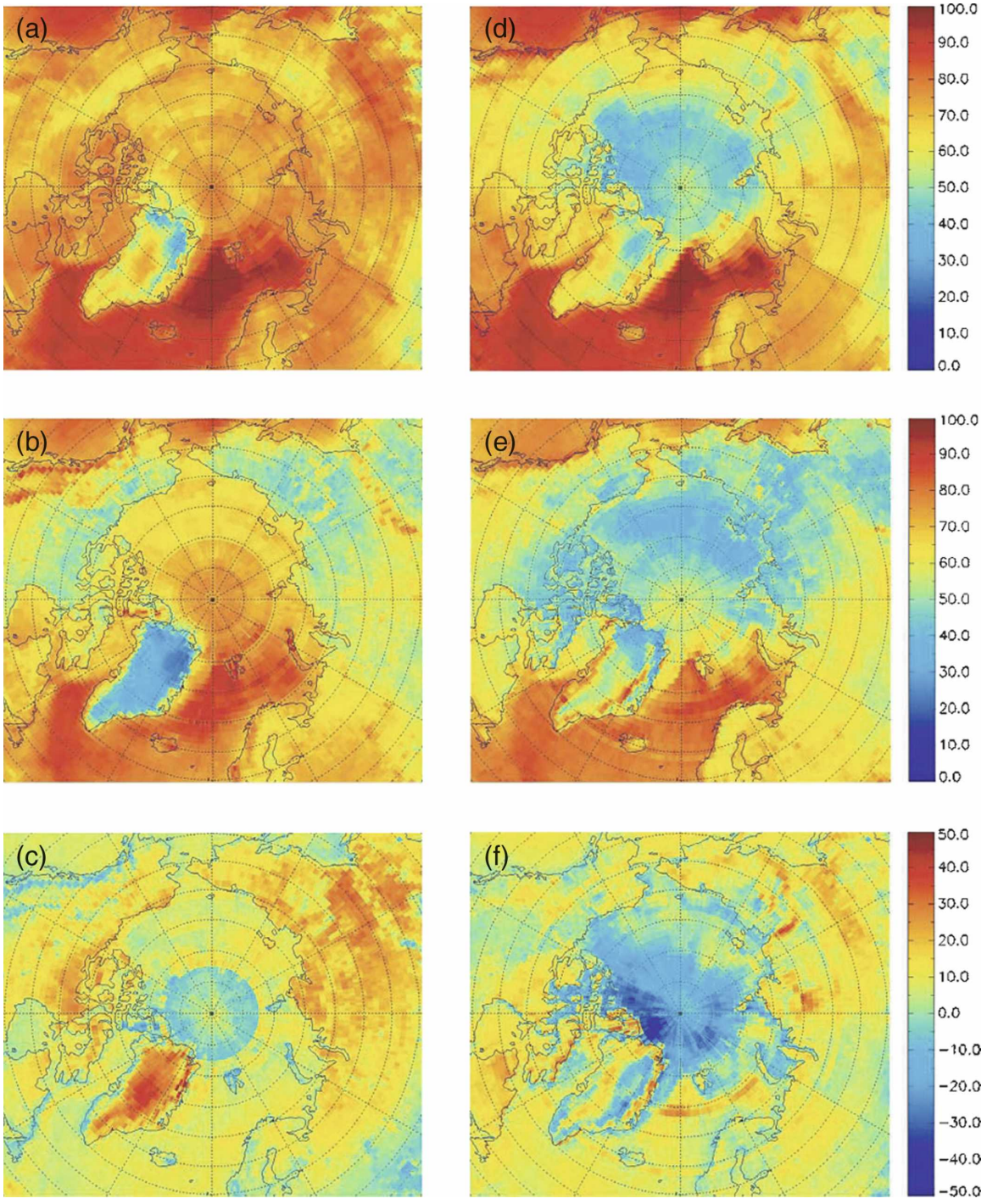

FIG. 3. Mean cloud frequency during January 2003–December 2004 for (a),(d) *Aqua* MODIS, (b),(e) APP-X, and (c),(f) MODIS minus APP-X during (left) daytime and (right) nighttime.

e. Nighttime ocean

Nighttime ocean cloud detection has undergone major changes. A sea surface temperature (SST) test and an 8.6–7.2-μm BTD test have been implemented for the first time. A new 11-μm BT variability test has also been included. The Reynolds SST (Reynolds and Smith 1994) minus 11-μm BTD test has the same function as the land surface temperature test, namely, as a gross cloud test. Because of more uniform ocean surface tem-

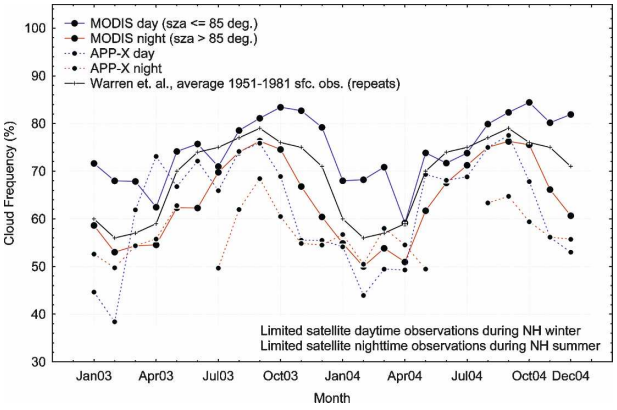

FIG. 4. Time series of *Aqua* MODIS and APP-X Arctic cloud frequencies for day and night conditions from January 2003–December 2004 (see legend). Warren et al. (1988) overall data from 1951–86 are shown for reference.

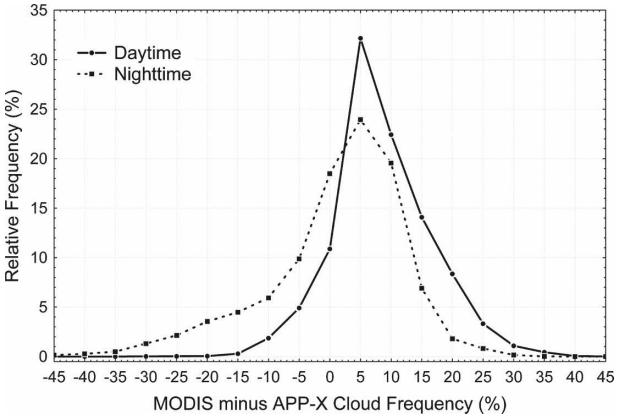

FIG. 5. Distributions of cloud frequency differences between *Aqua* MODIS and APP-X Arctic cloud frequencies for day and night conditions. Time period is January 2003–December 2004.

peratures, the threshold can be lowered to a base value of 6 K that is adjusted to account for viewing zenith angle and water vapor loading in the same way as described above for the land case.

An 8.6–7.2-μm BTD test has been added and is designed primarily to detect thick midlevel clouds but can also detect lower clouds in regions of low relative humidity in the middle atmosphere. It is sometimes more effective than the SST test for finding stratocumulus clouds of small horizontal extent. It can also detect high thick clouds. Both this and the SST test are needed to find those clouds that are thick but that also show very small thermal spatial variability. The test thresholds are 16.0, 17.0, and 18.0 K for 0.0, 0.5, and 1.0 confidence of clear sky, respectively.

The 11-μm variability test has been modified to detect clouds of small spatial extent (a pixel or two) and cloud edges. Most thick clouds are now found by other tests, but a variability test is very effective at night for detecting the thinner, warmer cloud edges over the uniform ocean surface. The previous (Collection 4) test determined a standard deviation over the pixel of interest and the eight surrounding pixels. Then, a very stringent threshold was used to determine cloudiness. In the Collection 5 version, the number of differences $\leq$0.5 K in 11-μm BT between each surrounding pixel and the center one are counted. The higher the number (8 possible), the more likely the center pixel is clear. The confident cloud and confident clear thresholds are 3 and 7, respectively. Figures 6a–d show example results from the above tests for an ocean scene with widespread stratus clouds in the subtropical southern Pacific west of South America.

The quality of the MODIS nighttime ocean cloud mask algorithm has seen a major improvement. The changes noted above have lowered the retrieved cloud amounts to reasonable levels and compare favorably with daytime values. This is a result of better detection of above-freezing clouds and use of less-stringent BT variability thresholds. Figure 7a shows zonal mean values of nighttime ocean clear-sky frequencies for one day from *Terra* Collection 4 and 5 algorithms. Though the locations of minima and maxima stay the same, clear-sky amounts increase by as much as 10% over the Southern Ocean and by as much as 20% over the northern subtropics.

To further investigate the quality and consistency of the nighttime ocean cloud mask, SSTs were computed and analyzed for the eastern Pacific ($-45°$ to $+45°$ latitude and 180° to 130°W longitude) over an 8-day period from 1 to 8 April 2003. Single-pixel values from day and night were calculated separately, then binned into 0.25-K histogram classes and compared with each other, as well as to the Reynolds SST data from the same locations and times. The current MODIS SST equation and coefficients (Brown et al. 1999) were used (but not the entire algorithm) along with clear-sky 11-μm BTs and 11–12-μm BTDs, where clear sky was determined solely from the C5 MODIS cloud mask (probably clear and confident clear designations). No 4-μm data were used at night and no preprocessing or postprocessing screening was performed except to eliminate obviously bad radiance data. The purpose of this exercise was not to produce the best SST possible, but rather to show that the ocean cloud mask performs well and is reasonably consistent between day and night. Figure 7b shows a histogram of SST values obtained for day and night in 0.25-K classes. The difference in the peak class between day and night is 0.25 K. Figure 7c shows a histogram with the same class widths but where

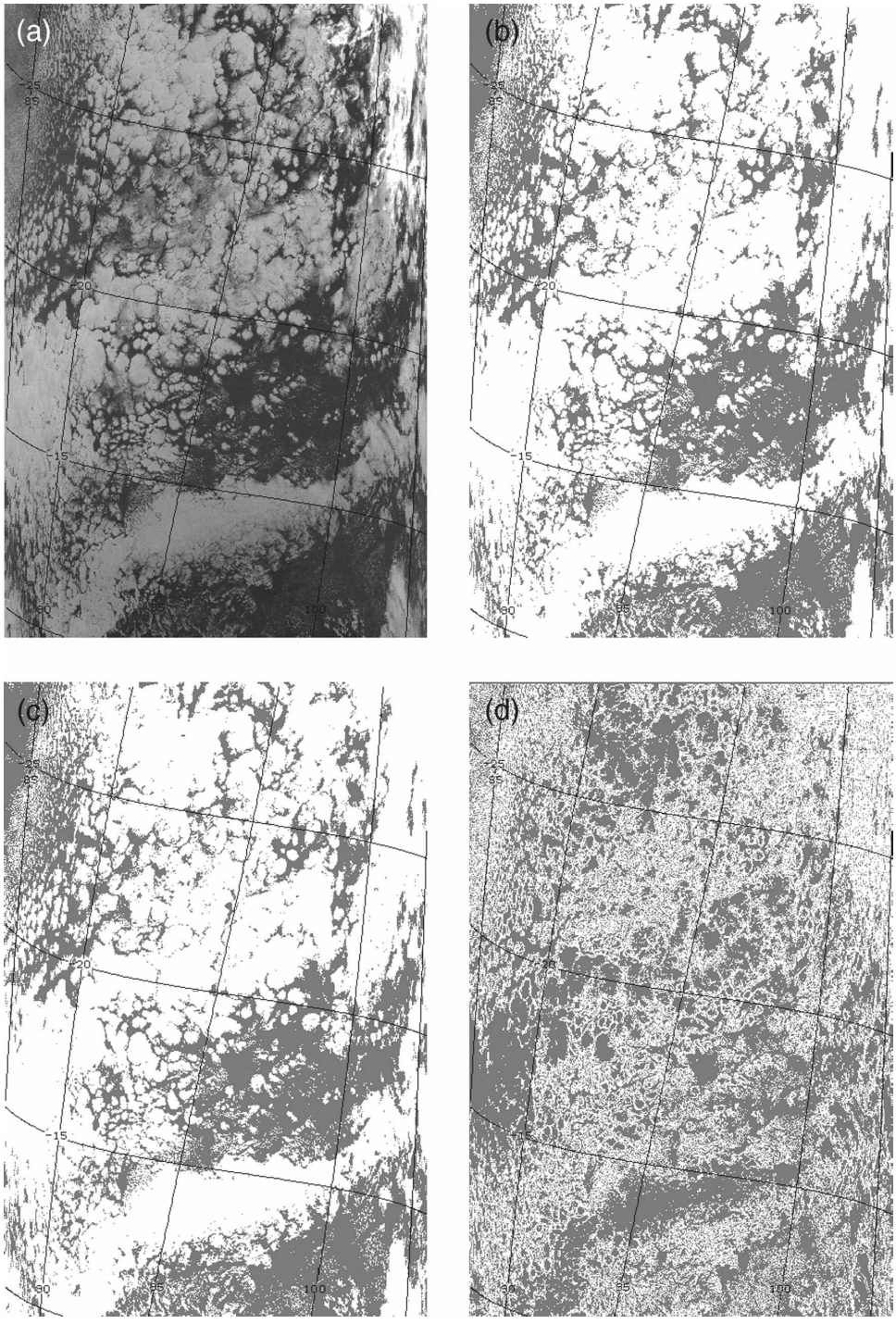

FIG. 6. Example scene of (a) MODIS 3.9-μm BT image, (b) SST test, (c) MODIS 8.6–7.2-μm BTD test, and (d) 11-μm variability test. Data are from 1900:10 UTC 6 Apr 2004.

the MODIS SSTs were compared to those of the Reynolds dataset. The Reynolds values did not change from day to night. The peak in the difference (MODIS − Reynolds) distribution lies at −0.25 K for both day and night, though there are less nighttime values for all difference classes warmer than the peak value and more for all less than the peak. This is undoubtedly mostly due to a little more cloud contamination in the nighttime clear-sky BTs, though direct observations of SST show a diurnal cycle of up to a degree or so in some

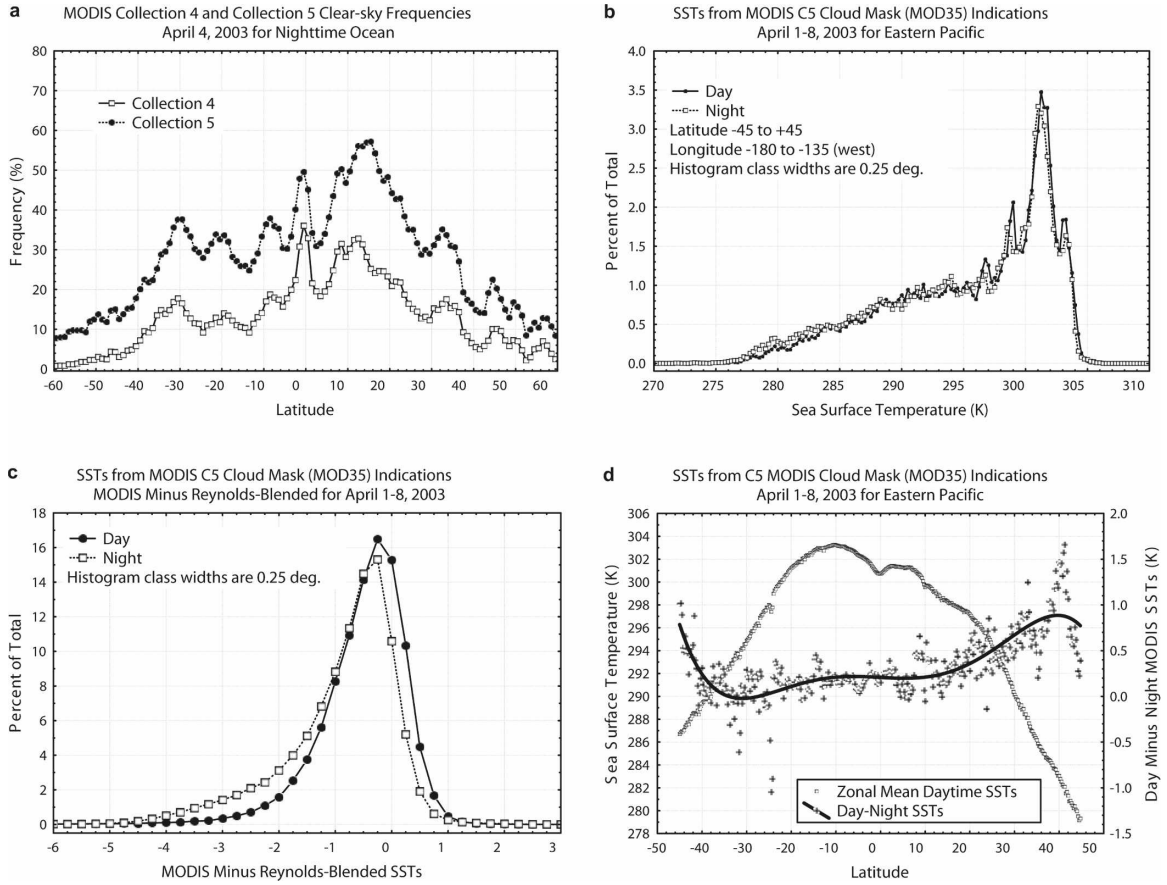

FIG. 7. (a) Zonal mean nighttime ocean clear-sky frequency from MODIS Collections 4 and 5 for 4 Apr 2003, (b) histogram of day and night SSTs using the same SST algorithm and coefficients, (c) histogram of MODIS vs Reynolds SSTs for day and night, and (d) zonal mean daytime SSTs and zonal mean day minus night SSTs. SST analysis uses data from the eastern Pacific Ocean ($-45°$ to $+45°$ latitude and $-180°$ to $-130°$ longitude). (b)–(d) Data are from 1–8 Apr 2003.

situations (Webster et al. 1996). Nevertheless, 82.1% of daytime and 68.6% of nighttime MODIS SSTs are within 1° of the Reynolds values on average, using nothing but MOD35 to determine the input BTs. Figure 7d shows the zonal mean daytime MODIS SSTs and day minus night differences (see Tables 1–3). The fit to the differences is a fifth-order polynomial. The larger zonal mean differences are seen in higher latitudes to both the north and south where more clouds are present and SSTs are lower. This is an indication that cloud edges are not as effectively screened out by the nighttime algorithm. One can see (in Fig. 9b) that, for the MOD35 algorithm, about 10% of ocean cloudy pixels are detectable only by use of visible and near-infrared (NIR) data.

Another exercise has compared SSTs generated from MODIS (MOD28) with those from the Advanced Microwave Scanning Radiometer for the Earth Observing System (AMSR-E) and Tropical Rainfall Measuring Mission (TRMM) Microwave Imager (TMI), but where differences are reported as functions of the MOD35 cloud categories. Global data including sun-glint and nighttime observations from 13 December 2006 were used. Figure 8 shows MODIS SSTs minus microwave SSTs from AMSR-E and TMI (MWSSTs) as functions of clear-sky confidence. Modal values of the differences in confident clear cases are -0.1 K for both day and night. Error values listed are percents of values < -2 K minus percents $> +2$ K for confident clear, probably clear, and probably cloudy. For confident cloud, error value is the percent between -2 and $+2$ K. As in Fig. 7, these histograms indicate that MOD35 is an effective cloud detection method during both day and night, but also that the four cloud mask output categories may be used as a kind of "quality flag" for derived products that rely heavily on unobstructed views of the surface.

f. Sun glint and daytime ocean

Improvements have been made to the cloud mask in sun-glint regions and in daytime oceans generally. The

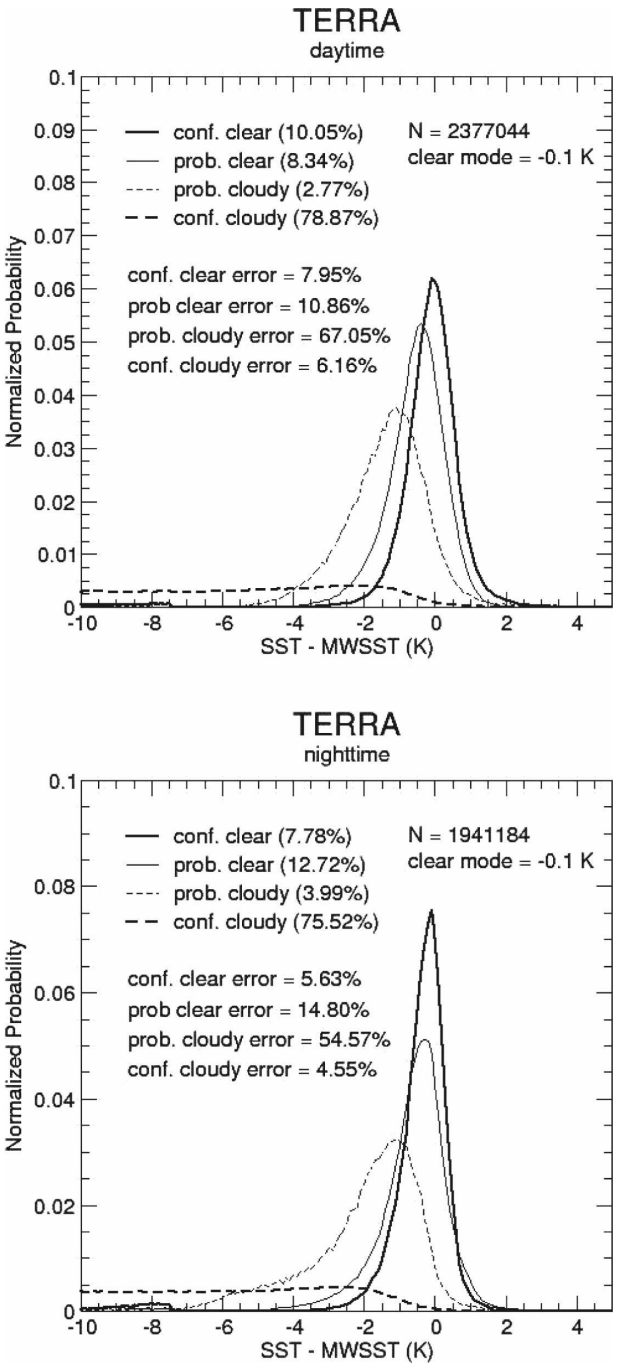

FIG. 8. Histograms of MODIS minus MWSST as functions of MOD35 clear-sky confidence levels: (top) daytime and (bottom) nighttime.

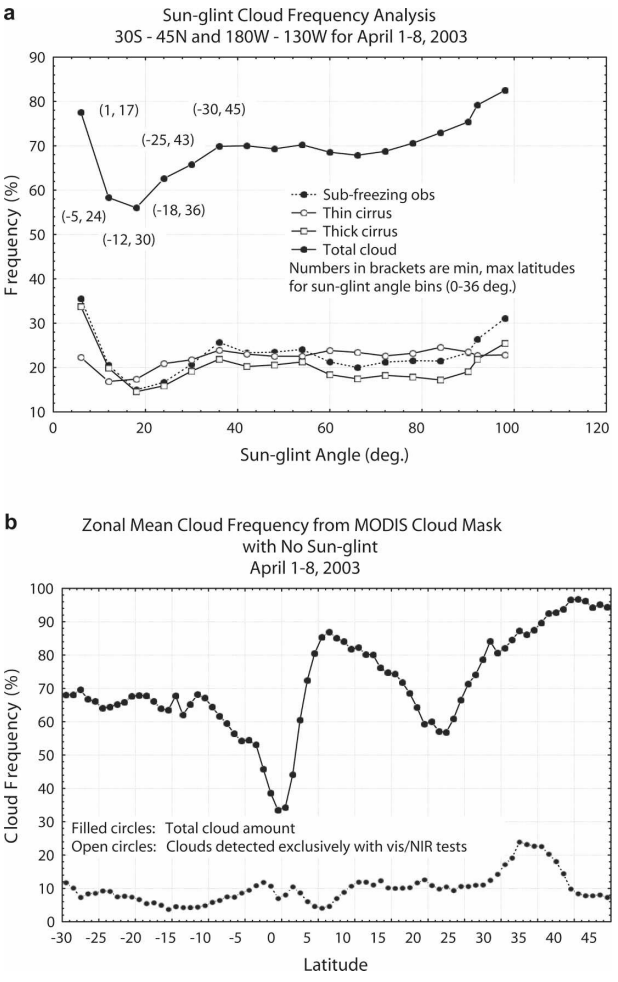

FIG. 9. Cloud frequencies as a function of (a) sun-glint angle and (b) latitude. The cloud frequencies in (b) do not contain any observations from sun-glint conditions. Data are from 1–8 Apr 2003.

SST test has been implemented in the daytime ocean algorithm exactly as in the nighttime case. For areas not affected by sun glint, the improvements are small since the algorithm has already been well developed for some time. The most noticeable change is more confident cloud and less uncertainty for scenes containing thin cirrus. The changes are more dramatic for areas affected by sun glint. Many low-level clouds with above-freezing cloud-top temperatures have been moved from the uncertain to the confident cloud category by use of the SST test. Much of the ambiguity between bright clouds and sometimes equally bright ocean surfaces, on the one hand, and between warm clouds and warm ocean surfaces, on the other hand, is ameliorated by knowledge of the SST.

In addition, a new clear-sky restoral test is applied. When no thermal tests indicate the presence of cloud, the mean and standard deviation of 0.86-μm reflectances (REFs) are computed over the pixel of interest and the eight surrounding. Pixels are declared to be probably clear (confidence 0.96) when the standard deviation multiplied by the mean is <0.001. This has the effect of restoring to clear many pixels that are bright in

TABLE 1. IR cloud test thresholds used in the MODIS cloud mask (MOD35) and the scene types for which the tests are applied. Linear interpolation is denoted by LI.

MODIS IR cloud test thresholds (MOD35)		
IR test	Thresholds for confidence limits (0.0, 0.5, 1.0, or low, middle, high)	Scenes
11 μm ("freezing" test)	267, 270, 273 K	All ocean
13.9 μm	222, 224, 226 K	All nonpolar
6.7 μm	215, 220, 225 K	All except Antarctic night
Surface temperature*–11 μm	6 K modified by VZA and 11–12-μm BTD +1 K/−2 K low/high**	Day, night deep ocean
Surface temperature–11 μm	Same as above, but base threshold=10 K	Day, night shallow ocean
Surface temperature–11 μm	12 K modified by VZA and 11–12-μm BTD ±2K low/high	Nonarid night land
Surface temperature–11 μm	20 K modified by VZA and 11–12-μm BTD ±2K low/high	Arid, semiarid night land
11–12-μm BTD	Function of VZA and 11-μm BT (Key 2002) Confidence limits vary by scene type, latitude	All except Antarctica
11, 12, 8.6 μm (trispectral test)	8.6–11-μm BTD threshold based on 11–12-μm BTD, ±0.5 K low/high	All ocean
11–3.9-μm BTD	−14, −12, −10 K	Nonarid day land
11–3.9-μm BTD	−20, −18, −16 K	Arid, semiarid day land 11-μm BT ≤ 320 K
11–3.9-μm BTD	10, 7, 4 K 14, 10, 6 K for elevations > 2000 m	Day snow/ice
11–3.9-μm BTD	11–12-μm BTD > +1.00: −2.0, −2.5, −3.0 K 11–12-μm BTD < −1.00: +5.0, +4.5, +4.0 K −1 ≤ 11–12-μm BTD ≤ +1 Linear interpolation (LI) between −2.5 and +4.5 K, ±0.5K low/high	Night land
11–3.9-μm BTD	0.7, 0.6, 0.5 K	Night snow/ice
11–3.9-μm BTD	−10, −8, −6 K	Day ocean
11–3.9-μm BTD	1.25, 1.00, −1.00 K	Night ocean
11–3.9-μm BTD	11-μm BT < 235 K: −0.1, −0.2, −0.3 K 11-μm BT > 265 K: +1.1, +1.0, +0.0 K 235 K ≤ 11-μm BT ≤ 265 K LI between −0.2 and +1.0 K, ±0.1 K low/high	Polar night land, snow/ice
11–3.9-μm BTD	11-μm BT < 230 K: −17.5, −14.5, −11.5 K 11-μm BT > 245 K: −10, −7, −4 K 230 K ≤ 11-μm BT ≤ 245 K LI between −14.5 and −7 K, ±3 K low/high	Polar day snow/ice 11-μm BT > 230 K
3.9–12-μm BTD	15, 10, 5 K	Night land
3.9–12-μm BTD	4.5, 4.0, 3.5 K	Night snow
3.9–12-μm BTD	11-μm BT < 235 K: 4.5, 4.0, 3.5K 11-μm BT > 265 K: 2.5, 2.0, 1.5 K 235 ≤ 11-μm BT ≤ 265 K LI between 4.0 and 2.0 K, ±0.5 K low/high	Polar night snow/ice (Elevation ≤ 2000 m)
7.2–11-μm BTD	−8, −10, −11 K	Night land, 11–3.9 μm ≤ −2 K
7.2–11-μm BTD	11-μm BT < 220 K: −1, 0, 1 K 220 K < 11-μm BT < 245 K LI between 0 K and −4.5 K, ±1 K low/high 245 K ≤ 11-μm BT < 255 K LI between −4.5 K and −10.5 K, ±1 K low/high 255 K ≤ 11-μm BT ≤ 265 K LI between −10.5 K and −20K, ±1 K low/high 11-μm BT > 265 K: −21, −20, −19 K	Polar night land, night snow
7.2–11-μm BTD	11-μm BT < 220 K: 0, 1, 2 K 220 K ≤ 11-μm BT < 245 K LI between 1 and −7 K, ±1 K low/high 245 K ≤ 11-μm BT < 255 K LI between −7 and −16.5 K, ±1 K low/high 255 K ≤ 11-μm BT ≤ 265 K	Night ice

TABLE 1. (*Continued*)

MODIS IR cloud test thresholds (MOD35)		
IR test	Thresholds for confidence limits (0.0, 0.5, 1.0, or low, middle, high)	Scenes
	LI between −16.5 and −20 K, ±1 K low/high 11-μm BT > 265 K: −21, −20, −19 K	
8.6–7.2-μm BTD	16, 17, 18 K	Night ocean 11 μm BT ≥ 280 K for polar night ocean
11-μm BT variability No. surrounding pixel BTs minus center pixel BT ≤ 0.5K	3, 6, 7	Night ocean

* Surface temperature is the surface temperature from ancillary data.
** Low/high is the low/high confidence of clear-sky thresholds for cloud tests.

the visible and NIR but also very uniform. This test is performed in addition to previously existing restoral tests.

To demonstrate the improvements in the cloud mask sun-glint algorithm and the consistency of results between sun-glint and non-sun-glint pixels, a region of the Pacific Ocean between −30° and +45° latitude was chosen for a detailed study. The longitudinal domain was −180° to −130° and the temporal range was 1–8 Apri1 2003. Figure 9a shows the total cloud amount as a function of glint angle binned in 6° increments. Sun glint is defined in the cloud mask algorithm as glint angles from 0° to 36°, where 0 defines the specular point (Ackerman et al. 1998). Because increasing sun-glint angles on the earth's surface are characterized by a series of concentric circles, larger glint angles also imply a wider range of latitudes, as well as increasing surface area and viewing zenith angles.

At first glance, the total cloud amount from the combined confident cloudy and uncertain decisions from MOD35 (top curve) would appear to be seriously biased in the sun-glint regions, but other indications of cloud (bottom curves) show the same pattern. Subfreezing observations in the 11-μm band are independent of sun glint, and thin and thick cirrus as determined by 1.38-μm reflectances are generally insensitive to glint in moist tropical regions. In addition, an L1b cross-talk calibration correction to this band removes most, if not all, of the sun-glint signal that might interfere with cloud detection in the drier subtropical areas characterized by atmospheric subsidence. The numbers in brackets along the top curve indicate the minimum and maximum latitudes from which the corresponding values originated.

Figure 9b shows total cloud frequency from the same region but from nonglint pixels and as a function of latitude. It can be seen from comparing the latitude ranges from the first plot to the cloud frequencies of those latitudes on the second that the trend toward lower cloud amounts in the latitudes most affected by glint is reasonable. Using the total number of observations from each glint angle bin as a surrogate for areal coverage (not exact), a reasonably accurate weighted average may be obtained over the entire region. The nonglint cloud amount was 70.8% while the cloud percentage from the glint region was 64.5%, a difference of 6.3%. Although not proven by this analysis, we suspect that the majority of missed cloudy pixels in glint areas are those warm clouds of small extent that would otherwise be detected exclusively by visible and NIR cloud tests. In areas affected by glint, the background ocean reflectance is often about the same or greater than that from these clouds, rendering them invisible. The bottom curve in Fig. 9b shows zonal means of the frequencies of these clouds as defined by the cloud mask from nonglint regions.

3. Conclusions

Changes for Collection 5 reprocessing in the MODIS cloud mask are described in this paper. They include changes in the polar night, ocean and land night, polar day snow, and sun-glint processing paths. Including tests for thin cirrus clouds (11–12- and 7.2–11-μm BTDs) will enhance the cloud detection capability in polar night conditions, while a new clear-sky restoral test (also 7.2–11-μm BTD) will allow more surface temperature inversions to be located that are normally cloud free. Users of the cloud mask will see an increase in the number of pixels flagged as cloudy under polar night conditions. The nighttime ocean algorithm has been reworked so that a more realistic amount of clouds is detected. Night ocean cloud amounts now compare well with those from daytime data. An analysis of SST using only MOD35 for cloud screening shows that a product that is very sensitive to small amounts of

TABLE 2. Visible (VIS) and NIR cloud test thresholds used in the MODIS cloud mask (MOD35) and the scene types for which the tests are applied.

MODIS VIS/NIR cloud test thresholds (MOD35)		
VIS/NIR test	Thresholds for confidence limits (0.0, 0.5, 1.0 or low, middle, high)	Scenes
0.86-μm REF	*Aqua* 0.065, 0.045, 0.030 *Terra* 0.055, 0.040, 0.030	Nonglint unfrozen day ocean
0.86-μm REF	0.34, 0.30, 0.26	Arid, semiarid day land (no snow)
0.86-μm REF	Glint angle 0°–10°: 0.115, 0.105, 0.095 Glint angle 10°–20° LI between 0.105 and 0.075, $\pm$0.01 low/high Glint angle 20°–36° LI between 0.075 and 0.045, $\pm$0.01 low/high (*Aqua*) LI between 0.075 and 0.040, $\pm$0.01 low/high (*Terra*)	Sun glint
0.66-μm REF	0.22, 0.18, 0.14	Nonsnow, nonarid day land
1.38-μm REF	0.040, 0.035, 0.030	Day scenes except snow/ice Elevation $\leq$ 2000 m
1.38-μm REF	0.0600, 0.0525, 0.0450	Day snow/ice Elevation $\leq$ 2000 m
0.86/0.66-μm REF ratio	0.95, 0.90, 0.85	Nonglint unfrozen day ocean
0.86/0.66-μm REF ratio	1.05, 1.00, 0.095	Sun glint
0.86/0.66 REF ratio [modified Global Environment Monitoring Index (GEMI)]	1.85, 1.90, 1.95	Noncoastal, nonarid day land (no snow)

cloud contamination generates reasonable results from both the day and night algorithms. It is not apparent that the nighttime SSTs show more cloud contamination than the daytime ones above that expected because of the lack of visible and NIR data. Zonal mean SST differences between day and night range from 0.25 K in the warmest regions to about 1 K in colder, cloudier areas. Day and night distributions of Reynolds SSTs versus SSTs using MOD35 peak at -0.25 K, with the Reynolds SST being warmer. A study of cloud amount as a function of sun-glint angle reveals that the cloud mask does a reasonable job in the difficult glint regions. An 8-day, area-weighted average of cloud amounts between glint and nonglint areas shows a deficit of 6.3% from glint regions. We suspect this difference is due to warm clouds of small areal extent that cannot be reliably detected by IR tests and that fade into the visible and NIR glint background reflectances. Users will see a marked decrease in false cloud determinations in daylight conditions during the spring and fall seasons in Greenland and Antarctica. This is due to a modification in the 3.9–11-μm BTD test.

Acknowledgments. The authors would like to graciously thank the MODIS science team, in particular P. Menzel, A. Heidinger, C. Moeller, B. Baum, C. Schaaf, M. King, V. Salmonson, and S. Platnick for their help in the development and testing of the MODIS cloud mask. This research was funded under NASA Grants NNG04HZ38C and NNG04GL14G; NNG04GB93G also contributed to this study. NOAA/NESDIS requires the following: "The views, opinions, and findings contained in this report are those of the author(s) and should not be construed as an official National Oceanic and Atmospheric Administration or U.S. Government position, policy, or decision." The authors continue to appreciate the support provided by the MODIS Characterization and Support Team and the MODIS Science Data Support Team. These research efforts have been supported by a number of agencies and research programs; a particular acknowledgement is due to the NASA Radiation Sciences Program and the NASA Earth Observing System Project Science Office.

APPENDIX

Cloud Mask Test Thresholds

Tables 1–3 list the IR and visible/NIR cloud test thresholds, and the clear-sky restoral test thresholds, respectively, used in the MODIS cloud mask. Values are the same for both *Terra* and *Aqua* instruments, unless indicated.

Individual cloud test thresholds have been developed

TABLE 3. Clear-sky restoral test thresholds used in the MODIS cloud mask (MOD35) and the scene types for which they are applied.

MODIS clear-sky restoral test thresholds (MOD35)		
Test	Threshold	Scenes
11-μm BT	*Aqua:* > 295.0 K, > 300.0 K, > 305.0 K	
	Terra: > 292.5 K, > 297.5 K, > 302.5 K	Day land, no snow, original confidence* $\leq$ 0.95
	Assign probably cloudy, probably clear, clear (thresholds adjusted for elevation)	No IR cloud tests positive
11-μm BT	*Aqua*: > 290.0 K, > 295.0 K, > 305.0 K	Nonvegetated land, no snow, original confidence $\leq$ 0.95, no IR cloud tests positive
	Terra: > 287.5 K, > 292.5 K, > 302.5 K	
	Assign probably cloudy, probably clear, clear (thresholds adjusted for elevation)	
0.55/1.24 μm	0.55/1.24 μm > 3.0 and 3.7–3.9-μm BTD < 11 K and 3.9–11-μm BTD < 15 K, assign probably clear	Day land, no snow, original confidence $\leq$ 0.95, no IR
3.7–3.9-μm BTD, 3.9–11-μm BTD		Cloud tests positive, above CSR tests Negative
11-μm BT	> 287.5 K, > 292.5 K, > 297.5 K	Nonpolar night land, no snow, original confidence $\leq$ 0.95
	Assign probably cloudy, probably clear, clear (thresholds adjusted for elevation)	No high- or middle-cloud tests positive
Normalized difference vegetation index	NDVI ≤ -0.18 or NDVI $\geq$ 0.40	Coast and shallow water
	Assign clear	No high- or middle-cloud tests positive
3.7–11-μm BTD	$\geq$ 13 K, assign probably cloudy	Sun glint, original confidence < 0.95, no high-, middle-, or surface temperature cloud tests positive
0.895/0.935 μm	> 3.0, assign probably clear	Same as above, positive 3.7–11-μm BTD test
0.86-μm REF	σ* mean < 0.001 over 3 × 3 pixel region, assign probably clear	Same as above, positive 3.7–11-μm BTD test
11-μm BT	8 surrounding pixels BTs minus center pixel BT $\leq$ 0.5 K, assign probably clear	Ocean, 0.66 < original confidence $\leq$ 0.95
11-μm BT	8 surrounding pixel BTs minus center pixel BT $\leq$ 0.5 K, assign probably cloudy	Ocean, 0.05 < original confidence $\leq$ 0.66
6.7–11-μm BTD	> +10 K, assign clear	Night snow
13.3–11-μm BTD	> +3 K, assign clear	Polar night snow
7.2–11-μm BTD	> +5 K, assign clear	Polar night snow

* Original confidence is the computed confidence of clear sky after all cloud tests performed.

in accordance with radiative transfer theory but "fine tuned" for specific surface and cloud types, and in some cases different instruments (*Aqua*, *Terra*). They are also calculated to be "clear-sky conservative." For the MODIS cloud mask, this means that each cloud test detects as many cloudy pixels as possible without generating unacceptable numbers of false positives in the final result. The final values are derived after testing many scenes in various seasons and under changing viewing geometries. Testing is also performed after any changes to the radiometric calibration of bands used in the cloud mask. In this sense, the tuned thresholds are empirical in nature.

Clear-sky restoral tests may override the computed confidence of clear sky in some cases. These are applied only after all cloud tests have been applied and combined to form a clear-sky confidence [Eqs. (1), (2) in the main text]. The need for these tests underscores the difficulty of *global* cloud detection, where pixel-by-pixel, regional and global, and temporal cloud statistics are required at high accuracy. There are three situations that are particularly problematic for global cloud detection algorithms: sun glint, unobstructed land surfaces that are as reflective as some clouds, and polar night conditions where little thermal contrast is present between surfaces and clouds. In the polar case, we look for evidence of deep atmospheric temperature inversions that indicate clouds are very unlikely. In sun-glint and bright land situations, unambiguous measures of clear sky are more difficult to define, but we use a combination of visible/NIR and IR tests that increases the confidence of clear sky when appropriate.

REFERENCES

Ackerman, S. A., K. I. Strabala, W. P. Menzel, R. A. Frey, C. C. Moeller, and L. E. Gumley, 1998: Discriminating clear-sky from clouds with MODIS. *J. Geophys. Res.,* **103** (D24), 32 141–32 157.

——, and Coauthors, 2006: Discriminating clear-sky from cloud with MODIS algorithm theoretical basis document (MOD35). 129 pp. [Available online at http://modis-atmos.gsfc.nasa.gov/_docs/MOD35:MYD35_ATBD_C005.pdf.]

Brown, O., P. Minnett, R. Evans, E. Kearns, K. Kilpatrick, A. Kumar, R. Sikorski, and A. Závody, 1999: Algorithm theoretical basis document. EOS ATBD. [Available online at http://modis.gsfc.nasa.gov/data/atbd/atbd_mod25.pdf.]

Derber, J., D. Parrish, and S. Lord, 1991: The new global operational analysis system at the National Meteorological Center. *Wea. Forecasting,* **6,** 538–547.

Key, J. R., 2002: The cloud and surface parameter retrieval (CASPR) system for polar AVHRR user's guide version 4.0. University of Wisconsin—Madison, 36 pp. [Available online at http://stratus.ssec.wisc.edu/caspr/userman.pdf.]

King, M. D., and Coauthors, 2003: Cloud and aerosol properties, precipitable water, and profiles of temperature and humidity from MODIS. *IEEE Trans. Geosci. Remote Sens.,* **41,** 442–458.

Liu, Y., J. Key, R. Frey, S. Ackerman, and W. Menzel, 2004: Nighttime polar cloud detection with MODIS. *Remote Sens. Environ.,* **92,** 181–194.

Platnick, S., M. D. King, S. A. Ackerman, W. P. Menzel, B. A. Baum, J. C. Riédi, and R. A. Frey, 2003: The MODIS cloud products: Algorithms and examples from Terra. *IEEE Trans. Geosci. Remote Sens.,* **41,** 459–473.

Reynolds, R., and T. Smith, 1994: Improved global sea surface temperature analyses. *J. Climate,* **7,** 929–948.

Saunders, R., and K. Kriebel, 1988: An improved method for detecting clear sky and cloudy radiances from AVHRR data. *Int. J. Remote Sens.,* **9,** 123–150.

Warren, S. G., C. J. Hahn, J. London, R. M. Chervin, and R. L. Jenne, 1986: Global distribution of total cloud cover and cloud type amounts over land. NCAR Tech. Note NCAR/TN 273+STR, 21 pp.+199 maps.

——, ——, ——, ——, and ——, 1988: Global distribution of total cloud cover and cloud type amounts over ocean. NCAR Tech. Note NCAR/TN 317+STR, 42 pp.+170 maps.

Webster, P. J., C. A. Clayson, and J. A. Curry, 1996: Clouds, radiation, and the diurnal cycle of sea surface temperature in the tropical western Pacific. *J. Climate,* **9,** 1712–1730.